Energy 36 (2011) 5877–5885

Contents lists available at SciVerse ScienceDirect

Energy

journal homepage: www.elsevier.com/locate/energy

Analysis of a 50 kW organic Rankine cycle system

Chi-Ron Kuo[a], Sung-Wei Hsu[a], Kai-Han Chang[b], Chi-Chuan Wang[b,*]

[a] Green Energy Research Laboratories, Industrial Technology Research Institute, Hsinchu 310, Taiwan
[b] Department of Mechanical Engineering, National Chiao Tung University, Hsinchu 300, Taiwan

ARTICLE INFO

Article history:
Received 12 July 2011
Received in revised form
21 August 2011
Accepted 23 August 2011
Available online 17 September 2011

Keywords:
Organic Rankine cycle
Thermal efficiency
Thermal resistance

ABSTRACT

This study analyzes the system performance of a 50 kW ORC system subject to influence of various working fluids. A dimensionless "figure of merit" combining the Jakob number, condensing temperature, and evaporation temperature is proposed for quantitatively screening working fluid as far as thermal efficiency is concerned. The thermal efficiency normally decreases with the rise of figure of merit, and the predictive ability of the proposed figure of merit is not only applicable to the present eighteen working fluids but is also in line with some existing literatures. Analysis of the typical ORC heat exchangers indicates that the dominant thermal resistance in the shell-and-tube condenser is on the shell side. Similarly, the dominant resistance is also on the refrigerant side for the plate evaporator. However, there is a huge difference of thermal resistance amid working fluid and water side in the preheating zone. Conversely, only a minor difference exists in the evaporation region. The extremely uneven resistance distribution in the plate heat exchanger can be resolved via an additional preheater having significant augmentation in the working fluid.

1. Introduction

The exploitation of low-grade heat has received growing interest due to the increased concern over energy shortage and global warming. There had been a number of new solutions proposed to generate electricity from the low-temperature heat sources. Among them, organic Rankine cycle (ORC) is a very potential candidate and is used in practical industrial applications such as biomass power, solar power, ocean thermal energy conversion (OTEC), geothermal power, waste heat recovery power. The ORC employs the same components in the conventional steam power plant, but use an organic fluid to extract low-grade thermal energy to generate electricity. Normally the temperature and pressure of the organic fluid is much lower than the 600 °C steam, thereby resulting in a much lower installation cost. The much lower temperature ORC system can be implemented comparatively simple with a single-stage expander rather than multi-stage turbines [1]. Yamamoto et al. [2] indicated that the cycle efficiency of working fluid is increased with the rise of pressure ratio rises. The authors also found that the R-123 working fluid shows a greater efficiency than that of water.

The system performance of ORC is strongly related to the working fluid. Hence it is essential to carefully select the appropriate working fluid. Hung et al. [3] showed that the major physical property of screening the working fluid includes specific heat, latent heat and slope of saturation vapor curve. According to the slope of saturation vapor curve in temperature–entropy diagram as shown in Fig. 1, the ORC fluid can be classified into (a) isentropic fluid: the slope of saturation vapor curve is infinite, such as R-11; (b) dry fluid: the slope of saturation vapor curve is positive, such as R-113 and benzene; (c) wet fluid: the slope of saturation vapor is negative, such as water and ammonia. Notice that the wet fluid is normally inappropriate for ORC system for concerns of entraining liquid droplet which is prone to damaging the turbine blade. Both the dry and isentropic fluid can lift the aforementioned severe disadvantage [4]. In addition, some other criteria for screening the working fluid are summarized as follows:

(a) The good working fluid should have a low liquid viscosity, a high liquid thermal conductivity, and a high latent heat of vaporization. These properties give a smaller system pressure drop as well as a higher heat transfer capacity.
(b) The good working fluid should have low specific volume. This property affects the input power and volume flow rate which is directly related to the cost of turbine [5].

* Corresponding author. Tel.: +886 3 5712121x55105; fax: +886 3 5720634.
E-mail address: ccwang@mail.nctu.edu.tw (C.-C. Wang).

0360-5442/$ – see front matter © 2011 Elsevier Ltd. All rights reserved.
doi:10.1016/j.energy.2011.08.035

Nomenclature

$\dot{W}$	power (kW)
$\dot{m}$	mass flow rate (kg/s)
v	specific volume (m^3/kg)
P	pressure (kPa)
$\dot{Q}$	heat transfer rate (kW)
i	specific enthalpy (kJ/kg)
Ja	Jacob number, dimensionless, $Ja = c_p\Delta T/i_{fg}$
U	overall heat transfer coefficient (W/m^2 K)
A	heat transfer area (m^2)
h	heat transfer coefficient (W/m^2 K)
R	thermal resistance (°C/W)
Nu	Nusselt number (hd/k)
f	friction factor
Re	Reynolds number ($\rho ud/\mu$)
Pr	Prandtl number
g	gravitational acceleration (m^2/s)
d	diameter (m)
u	velocity (m/s)
k	conductivity (W/m K)
T	temperature (°C)
N	number of tube row
Ge	non-dimensional geometric parameter
P_{co}	corrugation pitch (m)
Bo	boiling number
x	quality

Greek letters

η	efficiency
η_{th}	thermal efficiency
μ	viscosity (kg/m s)
β	chevron angle (radian)
ρ	density (kg/m^3)

Subscripts

wf	working fluid
p	pump
t	turbine (expander)
1, 2, 3, 4	states in system
id	isentropic
H	heat source
L	heat sink
w	water
G	gas
f	liquid
sat	saturated
fg	difference between liquid phase and gas phase
wall	wall
N	row of tube
Eq	equivalent
e	hydraulic

(c) The operating pressure should be kept as low as possible, higher operating pressure may lead to higher equipment cost. The suitable cycle pressure is around 0.1–2.5 MPa [6].
(d) The critical temperature should be higher than the maximum temperature of cycle. Organic fluid may suffer chemical decomposition and deterioration at a higher temperature or pressure [7].
(e) The working fluid should possess non-corrosive, non-toxic, non-flammable and environmentally friendly features.

The thermal efficiency of a system will vary with operating conditions. For dry fluid, the optimization of operating condition at the turbine inlet is saturated vapor. Normally it is not beneficial to operate at a superheat inlet condition [8]. Operating the turbine at a superheated state simply increases the condenser loading without increasing the output work. To improve the system efficiency, an internal heat exchanger (regenerator) is normally employed for lowering the superheat in the condenser, and extracting heat out of turbine outlet for preheating the working fluid in the evaporator [9].

In addition, there are other methods that can improve system performance, such as system operating optimization [10], combining feed-water heating [11], incorporating turbine bleeding [12], and integrating with other system techniques [13,14] etc.

There had been a number studies concerning ORC. Subjects include modeling for system performance, selection of an appropriate working fluid, improving system efficiency and second law efficiency, optimum design [9,10,15–19], and operational characteristics in supercritical region [9,20,21]. For an ORC system, heat exchangers (condenser and evaporator) play essential roles pertaining to system performance. Despite there were many studies associated with the design and analysis of ORC system, detailed designs within the heat exchangers were rarely found. As a result, one of the objectives of this study is to analyze the thermal resistance within these two heat exchangers (evaporator and condenser), and discuss possible improvements of the associated heat exchangers. A model ORC system with 50 kW capacity is used for detailed evaluation. In addition, the thermal efficiency of the ORC system performance is strongly to the working fluid. The aforementioned guideline for working fluid is simply qualitative, another objective of this study is to develop a "figure of merit" that is proven to be quite effective in quantitatively selecting the working fluid as far as thermal efficiency is concerned.

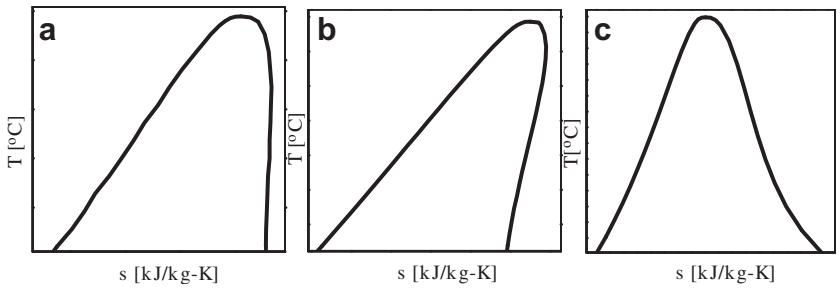

Fig. 1. The classification of working fluid (a) isentropic fluid; (b) dry fluid; and (c) wet fluid.

2. System and components modeling

The operating principle of ORC is similar to that of Rankine cycle, the system consists mainly of a pump, an evaporator, a turbine (expander) and a condenser as shown in Fig. 2. The pump delivers the working fluid into the evaporator where the working fluid vaporizes with supplied heat source. The existing high pressure vapor passes through the turbine and converts its kinetic energy into work. Finally the working fluid enters condenser to dissipate heat out of the working fluid and return to the pump to complete the cycle.

2.1. Calculation of system thermal efficiency

The major working fluids being investigated in this study include R-123, R-236fa, R-245fa, R-600, and n-Pentane. The basic properties of the working fluid are listed in Table 1. The analysis ignores the pressure loss from heat exchangers and piping. Further details of the mathematical model are given as follows:

Pump:

$$\dot{W}_p = \dot{m}_{wf} v_1 (P_2 - P_1)/\eta_p \quad (1)$$

Evaporator:

The heat exchange amid the evaporator is expressed as:

$$\dot{Q}_H = \dot{m}_{wf}(i_3 - i_2) \quad (2)$$

Expander:

$$\dot{W}_t = \dot{m}_{wf}(i_3 - i_{4,id})\eta_t \quad (3)$$

$$\eta_t = \frac{i_3 - i_4}{i_3 - i_{4,id}} \quad (4)$$

The subscript id denotes idea state.

Condenser:

Working fluid is condensed with heat exchange of cooling water, and the inlet temperature of cooling water is 30 °C.

The heat transfer rate in the condenser is given by:

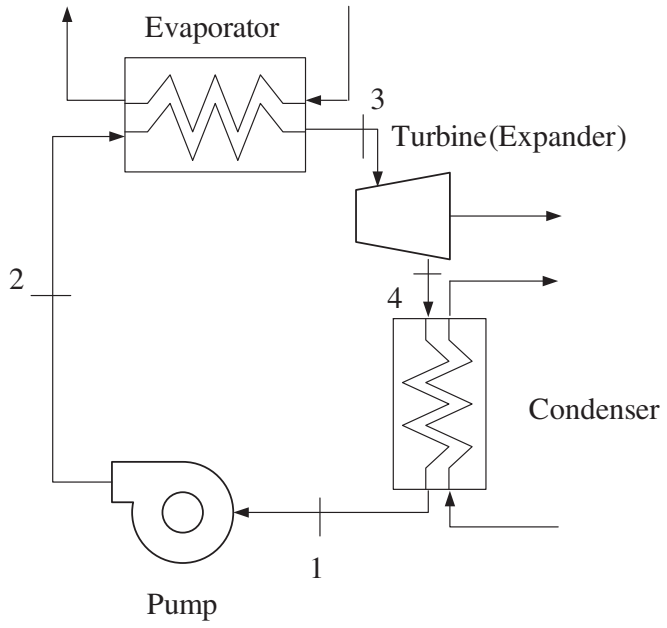

Fig. 2. The schematic diagram of an organic Rankine cycle.

Table 1
The basic characteristics of working fluid [30].

Working fluid	R-123	R-236fa	R-245fa	R-600	n-Pentane
Fluid type	Dry fluid	Dry fluid	Dry fluid	Dry fluid	Dry fluid
Critical temperature (°C)	183.68	124.92	154.01	151.98	196.55
Critical pressure (kPa)	3661.8	3200	3651	3796	3370
Normal boiling temperature (°C)	27.823	−1.44	15.14	−0.49	36.06
Molecular weight (kg/kmol)	152.93	152.04	134.05	58.122	72.149
ODP	0.02	0	0	0	0
GWP	77	9810	1030	~20	~20

$$\dot{Q}_L = \dot{m}_{wf}(i_4 - i_1) \quad (5)$$

The thermal efficiency is related to input power, output power and heat transfer rate.

$$\eta_{th} = \frac{\dot{W}_t - \dot{W}_p}{\dot{Q}_H} \quad (6)$$

The system performance is written using Engineering Equation Solver (EES). Details of the calculation procedures are outlined as follows:

1. From the prescribed condensing and evaporation temperatures, the associated physical properties at the condenser outlet and pump inlet are obtained.
2. The inlet state at the condenser is assumed to be at saturated vapor, hence the outlet state can be obtained after some iterations to meet the given turbine efficiency.
3. From the states of the operation points, the input evaporation heat, rejected heat from the condenser, output work, input work, and the system efficiency are therefore obtained.

2.2. Analysis of heat exchangers

In the present design, a plate heat exchanger (PHE) is incorporated as the evaporator whereas a shell-and-tube heat exchanger is used as the condenser. The cold and hot fluid flows alongside the plate channel counter-currently. Upon the PHE evaporator, both single-phase sensible heat transfer for preheating and two-phase evaporation occur. For the condenser, the working fluid flows on shell side and the cooling water flows on the tube side. For estimating the thermal resistance in these heat exchangers, the following empirical correlations are used:

2.2.1. Condenser

As seen in Fig. 3, the condenser is a four-pass design. And there are four tube rows in each path. The vapor entering from the top portion of the condenser and condenses along the tube bundle. The single-phase water flows in the tube side, and the heat transfer coefficient can be estimated from the Gnielinski correlation [22]:

$$Nu = \frac{\frac{f}{2}\cdot(Re - 1000)\cdot Pr}{1.07 + 12.7\sqrt{\frac{f}{2}\left(Pr^{\frac{2}{3}} - 1\right)}} \quad (7)$$

$$f = (1.58\ln Re - 3.28)^{-2} \quad (8)$$

During the condensation process, the outer wall surface temperature varies as the condensate film becomes thicker,

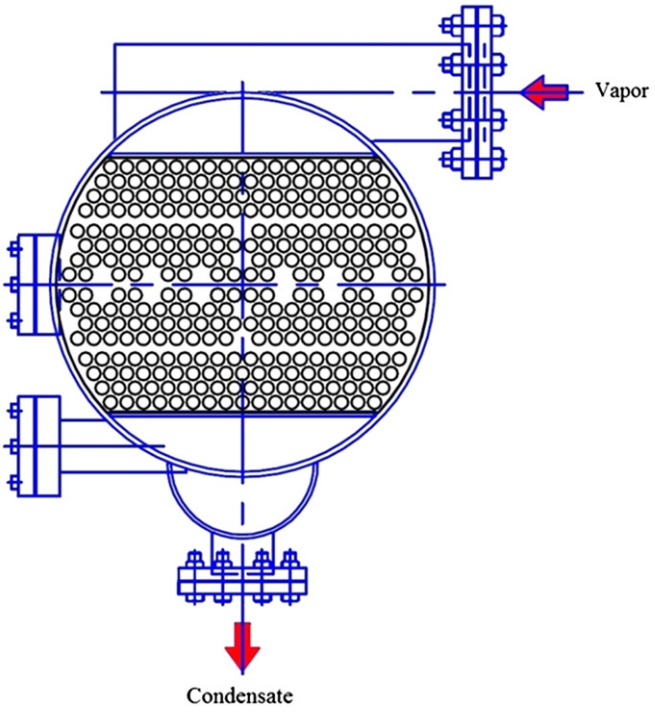

Fig. 3. Schematic of the condenser layout.

leading to a heat transfer deterioration alongside the tube row. Therefore it is essential to calculate the thermal resistance for each row.

The condensing heat transfer coefficients on the shell side for staggered arrangement subject to the influence vapor shear-and-tube row are taken from the Butterworth correlation [23] and Eissenberg correlation [24]:

$$\frac{Nu}{Re_G^{1/2}} = 0.416\left[1+\left(1+9.47\frac{gd\mu_f i_{fg}}{u_G^2 k_f (T_{sat}-T_{wall})}\right)^{0.5}\right]^{0.5} \tag{9}$$

$$\frac{h_N}{h} = 0.6 + 0.42N^{-\frac{1}{4}} \tag{10}$$

The overall heat transfer coefficient is as follows:

$$\frac{1}{UA} = \frac{1}{h_{wf}A_{wf}} + \frac{1}{h_w A_w} + R_{wall} \tag{11}$$

where h_{wf} and h_w represent the heat transfer coefficients on shell-and-tube side, respectively. R_{wall} is the tube wall resistance.

2.2.2. Evaporator

The plate heat exchanger is divided into a preheating and an evaporation region, therefore it is needed to include both single- and two-phase correlations for analyzing the plate heat exchanger. For the single-phase heat transfer correlation, the Kim correlation [25] is used:

$$Nu = 0.295Re^{0.64}Pr^{0.32}\left(\frac{\pi}{2}-\beta\right)^{0.09} \tag{12}$$

For the two-phase evaporation heat transfer performance, the correlation developed by Han et al. [26] is adopted:

$$Nu = Ge_1 Re_{Eq}^{Ge_2} Bo_{Eq}^{0.3} Pr^{0.4} \tag{13}$$

where

$$Ge_1 = 2.81\left(\frac{P_{co}}{D_e}\right)^{-0.041}\left(\frac{\pi}{2}-\beta\right)^{-2.83} \tag{14}$$

$$Ge_2 = 0.746\left(\frac{P_{co}}{D_e}\right)^{-0.082}\left(\frac{\pi}{2}-\beta\right)^{0.61} \tag{15}$$

3. Results and discussion

3.1. Screening of working fluid and derivation of figure of merit

In general, it is improbable to use only one property to screen out the working fluid. This is because the system efficiency is affected by many specific thermophysical properties. For further elaborating the influence of thermophysical properties on the system performance, calculation is made with eighteen working fluids using some physical properties suggested from some researchers, including the critical temperature [9], normal boiling point [5], latent heat [3], molar mass [27] and specific heat [28]. The calculation is shown in Fig. 4 and is conducted with evaporation temperatures of 130 °C and 80 °C at a fixed condensation temperature of 45 °C. Apparently none of the sole physical property can justify itself as the best indicator as far as the thermal efficiency is concerned. In fact, appreciable inconsistencies are encountered when using latent heat, molar mass, or specific heat. In the meantime, though the critical temperature or the normal boiling point gives a fair screening with a rising tendency of thermal efficiency. However, some evident fluctuation exists amid the examined working fluids, suggesting insufficient ability of these two properties to screen out the working fluids. In summary of the foregoing discussion, it is therefore concluded that no single physical property can be used as the sole indicator for quantitatively screening the working fluid.

For typical ORC operation, the heat input into the evaporator includes sensible heat and latent heat. In this study, we find that the Jacob number, charactering as the ratio of the sensible heat transfer and the latent heat of evaporation, defined as $Ja = c_p\Delta T/i_{fg}$, plays an essential role to discriminate the thermal efficiency amid various working fluids. Notice that c_p represents the average specific heat evaluated from the mathematical mean of the condensing and evaporating temperature, ΔT is the temperature difference between evaporation and condensation, whereas i_{fg} denotes the latent heat of evaporation temperature. For different working fluids operated at the same condensing and evaporation temperatures, as shown in Fig. 5(a), it is found that a lower value of *Ja* results in a higher thermal efficiency, and this indicator can be used as a screening parameter amid different working fluids. The tendency prevails pertaining to various condensing temperatures (Fig. 5(b)) and evaporation temperatures (Fig. 5(c)). However, it should be emphasized that the *Ja* number can only be used as a screening indicator between different working fluids, it is not applicable for the same working fluid operated at different condensing or evaporating temperatures. To tailor this inconsistency, a modified dimensionless "figure of merit" is proposed in the following

$$\text{Figure of Merit (FOM)} = Ja^{0.1}\left(\frac{T_{cond}}{T_{evap}}\right)^{0.8} \tag{16}$$

Fig. 5(d) shows the thermal efficiency subject to various condensing temperatures and evaporation temperatures with the proposed FOM. It can be seen that the thermal efficiency decreases consecutively with the proposed FOM for all the eighteen working fluids. For further substantiating the proposed FOM as the

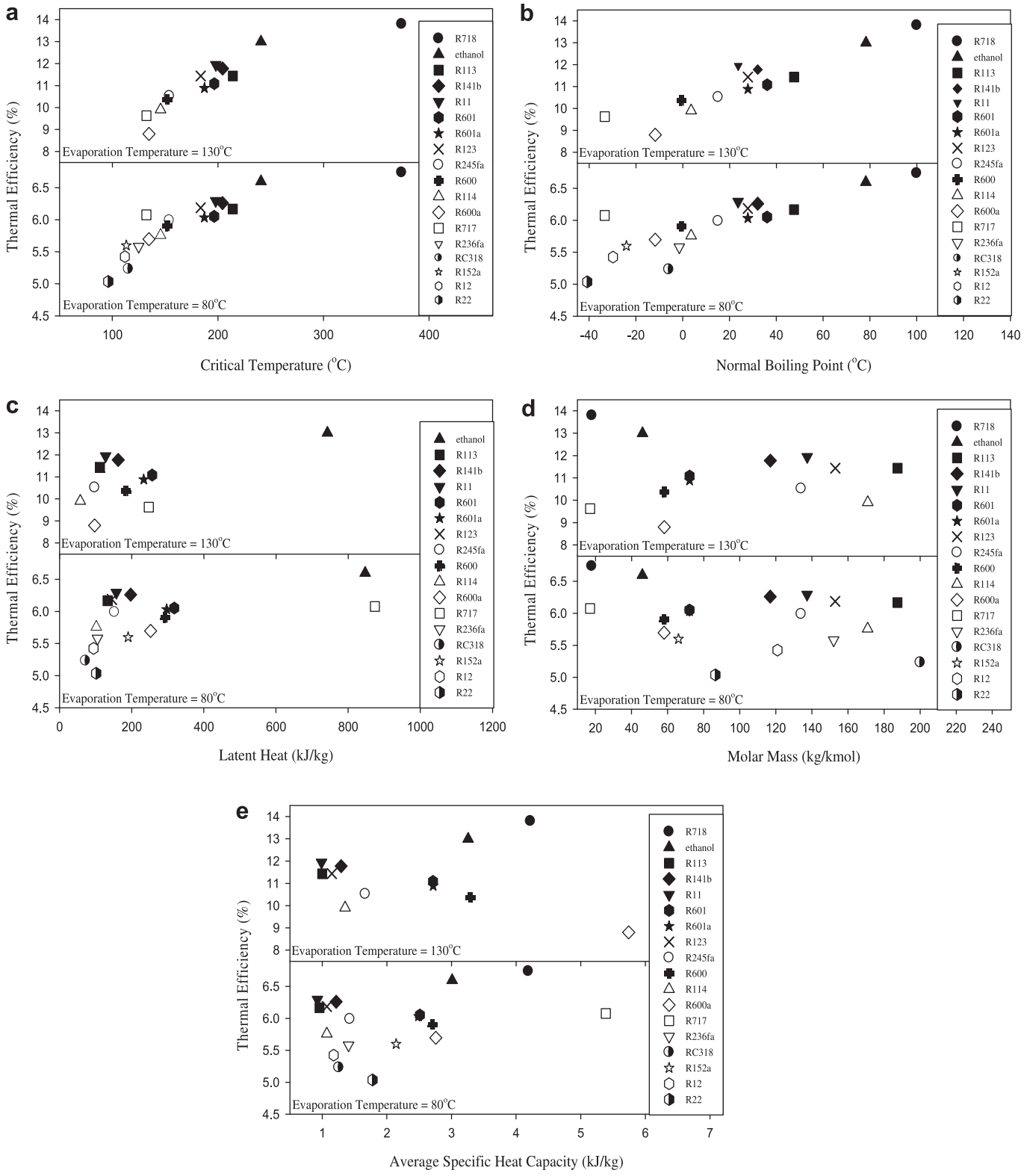

Fig. 4. Influence of physical properties on the thermal efficiency (a) critical temperature; (b) normal boiling point; (c) latent heat at evaporation temperature; (d) molar mass; and (e) specific heat.

quantitatively screening parameter, the proposed FOM is also compared with some existing literatures [5,9]. Fig. 6 shows excellent agreements between the calculated results from [5,9] vs. the proposed FOM. In essence, the proposed FOM can be used to discriminate the working fluids based on the thermal efficiency.

3.2. The system performance of the 50 kW system

Fig. 7 shows the comparison in terms of the thermal efficiency amid R-123, R-236fa, R-245fa, R-600 and n-Pentane for a 50 kW ORC system. The calculation is conducted with a corresponding

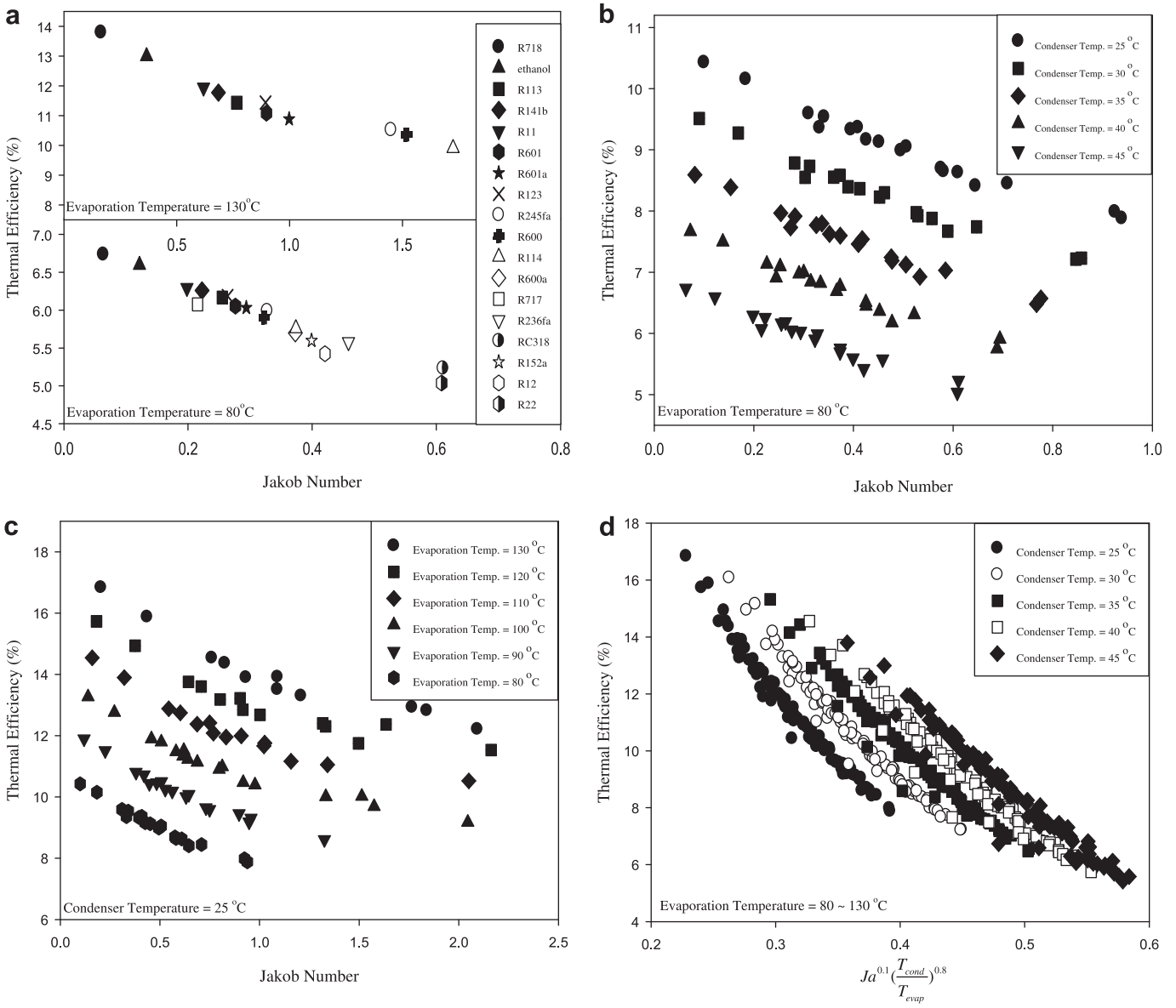

Fig. 5. Influence of evaporation temperature and condensation temperature on thermal efficiency for (a) various working fluids at evaporation temperatures of 130 °C and 80 °C with condensing temperature of 45 °C; (b) varying condensing temperature; (c) varying evaporation temperature; and (d) combined influences of condensing and evaporation temperatures.

evaporation temperature of 108 °C and a condensing temperature of 45 °C. The pump efficiency is 0.65 and the expander efficiency is 0.7. The cooling water temperature at the condenser inlet is 30 °C whereas the hot water inlet temperature at the evaporator is 125 °C. The inlet of the expander can be operated at the two-phase region while the outlet state of the expander is in the saturated vapor state. In the simulation, the inlet quality of expander varies with operating condition of working fluid. As seen in Fig. 7, the system thermal efficiency increases with the evaporation temperature. It is found the highest thermal efficiency is R-123, followed by n-Pentane, R-245fa, R-600, and R-236fa. Notice that the calculation is made with a prescribed output of 50 kW. As seen in the figure, it seems that the thermal efficiency is in line with rise of the latent heat of vaporization. Hung et al. [3] had investigated eleven working fluids on the ORC system efficiency, and they found that three thermophysical properties, namely the slope of the saturation curve, specific heat, and latent heat, cast major influence on the thermal efficiency. Among these three properties, Hung et al. [3] indicated that working fluid with higher latent heat often outperforms those with lower latent heat. However, they also reported some inconsistency, for example R-152a has a comparatively high latent heat but normally shows the least system efficiency. Analogous inconsistency about the influence of latent heat on system efficiency was also reported in Tchanche et al.'s survey [5] for working fluids applicable for low-temperature solar ORC. The thermal efficiency normally increases with the rise of evaporation temperature, and it is usually expected that the tendency persists as the temperature is increased above critical point. This is associated with the fact that the average high temperature for supplied heat is higher than the subcritical process [29]. However, in practice, a significant increase of heat exchanger surface is required for gas heating in the supercritical region. The supercritical Rankine cycle involves a heating process without a distinct two-phase region, thereby resulting in a better thermal match with less irreversibility [20]. Also, the so-called pinching problem which may occur in ORC counter-current heat exchanger can be avoided through

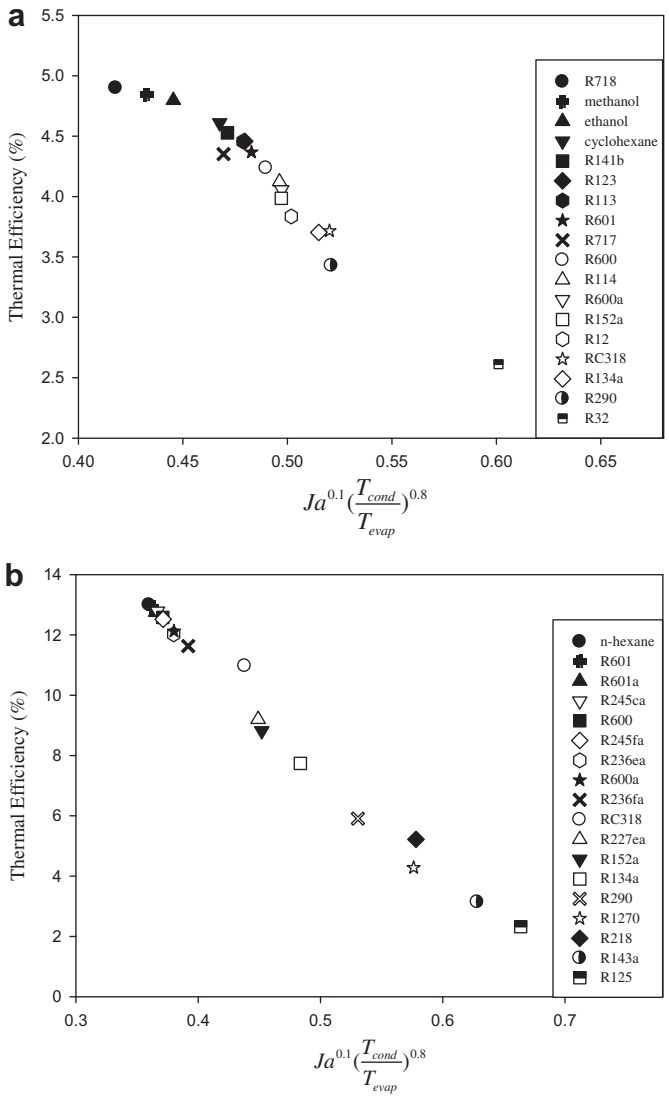

Fig. 6. Calculated thermal efficiency from references of (a) [5]; and (b) [9] vs. the proposed figure of merit $(Ja^{0.1}(T_{cond}/T_{evap})^{0.8})$.

Table 2
The thermal efficiency of variation inlet turbine temperature with different operating pressures.

T_3 (°C)	P_3 (kPa)	h_2 (kJ/kg)	h_3 (kJ/kg)	h_4 (kJ/kg)	W_{net} (kW)	Q_H (kW)	η
156	3700	263.5	484.5	455.5	24.9	221	11.27
	3900	263.7	447.2	424.7	18.14	183.5	9.89
	4100	264	442	420.3	17.11	178.1	9.61
	4300	264.2	439.4	418.1	16.53	175.2	9.44
160	3700	263.5	500.9	469.3	27.6	237.5	11.62
	3900	263.7	488.2	458.3	25.6	224.5	11.4
	4100	264	463.4	437.8	21.04	199.4	10.55
	4300	264.2	452.8	429	19	188.6	10.07
180	3700	263.5	541.4	503.9	33.4	277.9	12.02
	3900	263.7	537.7	500.2	33.2	274	12.11
	4100	264	533.7	496.3	32.87	269.8	12.18
	4300	264.2	529.3	492.1	32.41	265.1	12.22

supercritical operation [29]. On the downside, the organic fluid is normally not recommended to operate in the supercritical region due to the risk of chemical decomposition and corrosion problem. In the present study, a typical calculation concerning the operation beyond supercritical region is made for R-245fa (the critical temperature is 156 °C) and the calculated results are tabulated in Table 2. Comparing with those ORC being operated at the subcritical region, the thermal efficiency for supercritical operation is normally higher than that of the subcritical operation by about 5–10%. And this phenomenon is especially pronounced at a more elevated temperature. However, at a given expander inlet temperature, elevating the pressure often leads to a drop of system performance as seen in Table 2. Yet the phenomenon becomes more severe when the temperature approaches the critical temperature. This is because the isobar line changes dramatically near the critical point, and a sharp variation of the corresponding enthalpy. In the meantime, the efficiency shows a plateau against the pressure. For example, the thermal efficiency of R-245fa peaks at a turbine inlet temperature of 156 °C and a pressure of 3700 kPa. The results can be further made clear from Fig. 8 where the isobar line varies appreciably when varying the pressure from 3700 kPa to 3800 kPa, leading to a considerable drop of thermal efficiency. By contrast, with a rise of the turbine inlet temperature to 180 °C, the thermal efficiency rises slightly with the pressure due to comparatively small variation of isenthalpic line.

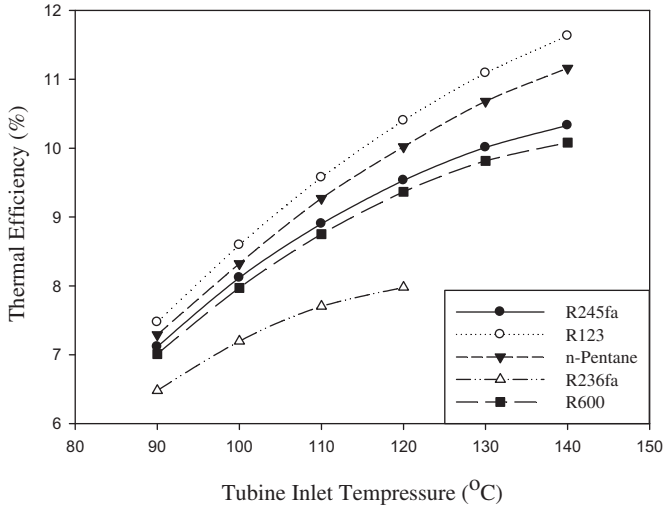

Fig. 7. The variation of thermal efficiency with evaporation temperature for different working fluids.

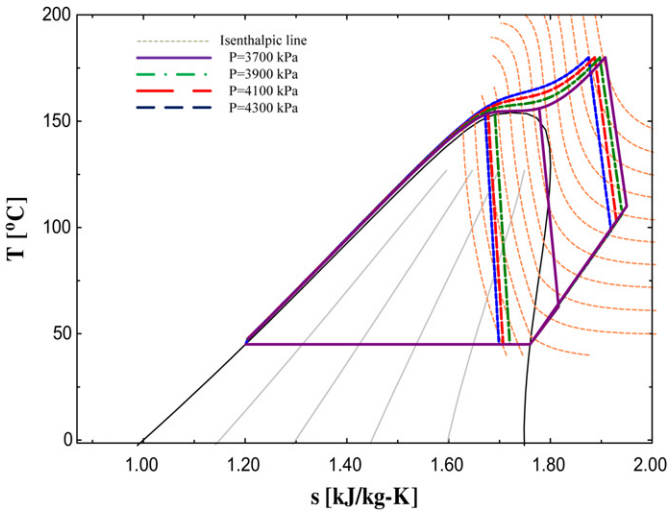

Fig. 8. The T–S diagram with various turbine inlet pressures.

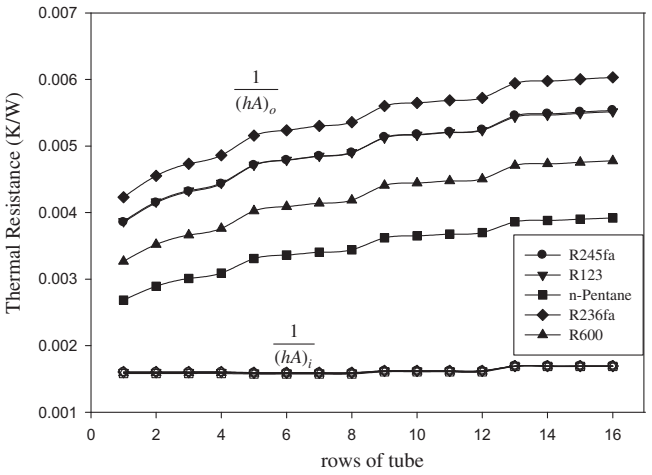

Fig. 9. The distribution of thermal resistance for condenser with different working fluids.

3.3. Analysis of the thermal resistance amid heat exchangers

As mentioned in the condenser design that the condensate film thickness increases alongside the tube row as condensation takes place. This eventually leads to a drop of condensation heat transfer coefficient. Fig. 9 depicts the variation of the tube side and shell side thermal resistance within the condenser. It appears that the tube side thermal resistance remains almost unchanged whereas an appreciable rise of thermal resistance with the tube row on the shell side is encountered. And the dominant thermal resistance occurs at the shell side. The calculated results indicate that the largest thermal resistance is R-236fa, followed by R-245fa, R-123, R-600 and the n-Pentane. The thermal resistance for R-123 and R-245fa is nearly equal. For improving the overall performance, using enhanced tubes like low fin tubes may be beneficial and is applicable for all the working fluids especially for R-236fa. For example, for the same operating parameters and capacity, the surface area of condenser can be reduce as much as 35% for R-245fa refrigerant provided that the condensing heat transfer coefficient is augmented by 100%.

Similar estimations of the thermal resistance along the evaporator are also performed as seen in Fig. 10. Heat transfer within the evaporator for working fluid can be classified as preheating (single-phase) and convective evaporation (two-phase). For the preheating region (Fig. 10a), the dominant thermal resistance is clearly on the refrigerant side. Note that the difference is more than an order of magnitude, indicating a highly insufficient design for the single-phase heat transfer of the working fluid. On the other hand, the difference in thermal resistance amid working fluid in the two-phase region and water (Fig. 10b) is generally much smaller than that in the preheating region irrespective of higher thermal resistance still persists in the working fluid side. The results imply a very difficult situation for effective improvements in the plate heat exchanger for one needs substantial improvements in the preheating region while only very minor improvements at the two-phase region are required. This is because it is not practical to impose a significant difference of the plate geometry from entry to exit. Hence, a better design is to employ a separate preheater with a significant augmentation in the refrigerant side. Through this modification, the original size of the plate heat exchanger can be appreciably reduced for incorporating two-phase evaporation.

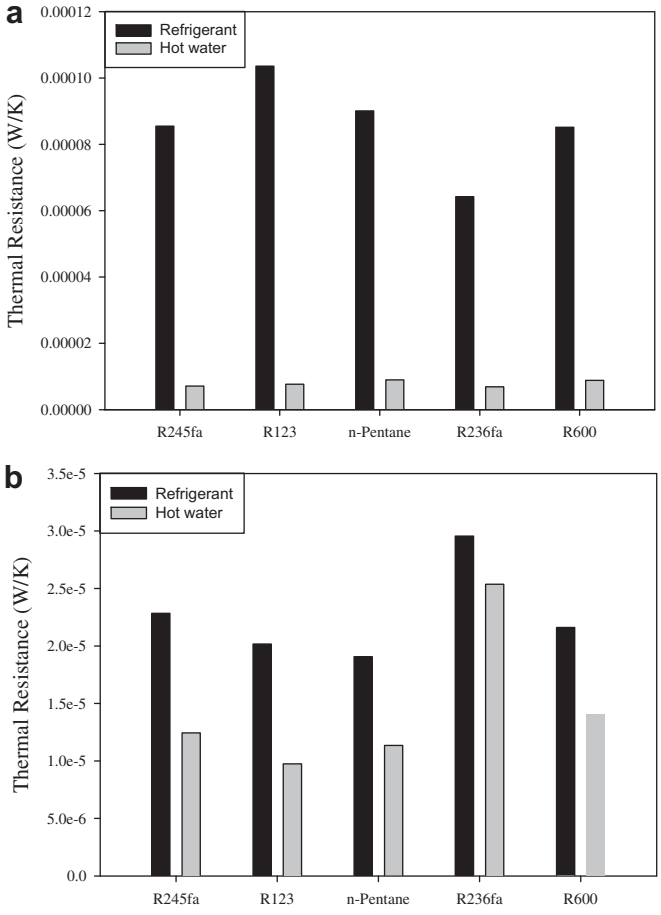

Fig. 10. The thermal resistance for different working fluids in (a) single-phase preheating region; and (b) two-phase evaporation region.

4. Conclusions

This study analyzes the system performance of a 50 kW ORC system subject to various working fluids. The thermal efficiency of an ORC system is strongly related to thermophysical properties. However, there is no single thermophysical property that can be used as the best indicator for screening the working fluids as far as thermal efficiency is concerned. The present authors propose a Jacob number which is termed as the ratio of the sensible heat transfer and the latent heat of evaporation. The Jacob number can discriminate the thermal efficiency amid various working fluids. And the Jacob number can be further combined with the ratio of condensing temperature and evaporation temperature to form a “figure of merit” that is proved to be very effective screen the working fluid at various condensing/evaporation temperatures as far as thermal efficiency is concerned. The thermal efficiency normally decreases with the rise of figure of merit. The proposed figure of merit is not only applicable for the present eighteen working fluids but is also in line with some existing literatures.

The present study also examines the thermal efficiency subject to supercritical operation. Depending on the pressure, the thermal efficiency for supercritical operation is normally higher than that of subcritical operation by about 5–10%. And this phenomenon becomes more pronounced at a more elevated temperature. However, at a given expander inlet temperature, elevating the pressure often leads to a drop of system performance. Yet the phenomenon becomes especially severe when the temperature approaches the critical temperature. This is because the isobar line changes dramatically near the critical point, and a sharp variation of the corresponding enthalpy. In the meantime, the thermal efficiency shows a plateau with increasing the pressure.

For the analysis of the shell-and-tube condenser subject to operating conditions, the results indicate that the dominant thermal resistance is always on the shell side. Hence using enhanced heat transfer tubes such as low finned tubes can effectively improve the overall performance. Similarly, it is found that the dominant resistance is also on the working fluid side of the plate evaporator. However, there is a huge difference of thermal resistance in the preheating zone whereas only a minor difference exists in the evaporation regime. The result implies a difficult situation for effective heat transfer augmentation. A better way to tackle this problem is to use a separate preheater heat exchanger incorporating significant augmentation in the working fluid side. With this design, the size of the original plate heat exchanger can be appreciably reduced.

Acknowledgments

The authors would like to express gratitude for the Energy R&D foundation funding from the Bureau of Energy of the Ministry of Economic, Taiwan and National Science Committee of Taiwan (under contract 100-ET-E-009-004-ET).

References

[1] Badr O, Probert SD, O'Callaghan PW. Selecting a working fluid for a Rankine-cycle engine. Applied Energy 1985;21:1–42.
[2] Yamamoto T, Furuhata T, Arai N, Mori K. Design and testing of the organic Rankine cycle. Energy 2001;26:239–51.
[3] Hung TC, Wang SK, Kuo CH, Pei BS, Tsai KF. A study of organic working fluids on system efficiency of an ORC using low-grade energy sources. Energy 2010; 35:1403–11.
[4] Liu BT, Chien KH, Wang CC. Effect of working fluids on organic Rankine cycle for waste heat recovery. Energy 2004;29:1207–17.
[5] Tchanche BF, Papadakis G, Lambrinos G, Frangoudakis A. Fluid selection for a low-temperature solar organic Rankine cycle. Applied Thermal Engineering 2009;29:2468–76.
[6] Maizza V, Maizza A. Unconventional working fluids in organic Rankine-cycles for waste energy recovery systems. Applied Thermal Engineering 2001;21:381–90.
[7] Hung TC, Shai TY, Wang SK. A review of organic Rankine cycles (ORCs) for the recovery of low-grade waste heat. Energy 1997;22:661–7.
[8] Mago PJ, Chamra LM, Somayaji C. Performance analysis of different working fluids for use in organic Rankine cycles. Proceedings of the Institution of Mechanical Engineers, Part A: Journal of Power and Energy 2007;221:255–63.
[9] Saleh B, Koglbauer G, Wendland M, Fischer J. Working fluids for low-temperature organic Rankine cycles. Energy 2007;32:1210–21.
[10] Wei L, Zhang Y, Mu Y, Yang X, Chen X. Efficiency improving strategies of low-temperature heat conversion systems using organic Rankine cycles: an overview. Energy Sources, Part A: Recovery, Utilization, and Environmental Effects 2011;33(9):869–78.
[11] Mago PJ, Chamra LM, Srinivasan K, Somayaji C. An examination of regenerative organic Rankine cycles using dry fluids. Applied Thermal Engineering 2008;28:998–1007.
[12] Desai NB, Bandyopadhyay S. Process integration of organic Rankine cycle. Energy 2009;34:1674–86.
[13] Tamm G, Goswami DY, Lu S, Hasan AA. Theoretical and experimental investigation of an ammonia–water power and refrigeration thermodynamic cycle. Solar Energy 2004;76:217–28.
[14] Zhang XR, Yamaguchi H, Uneno D, Fujima K, Enomotoc M, Sawadaddioxide N. Analysis of a novel solar energy-powered Rankine cycle for combined power and heat generation using supercritical carbon dioxide. Renewable Energy 2006;31:1839–54.
[15] Hung TC. Waste heat recovery of organic Rankine cycle using dry fluid. Energy Conversion and Management 2001;42:539–53.
[16] Papadopoulos AI, Stijepovic M, Linke P. On the systematic design and selection of optimal working fluids for organic Rankine cycles. Applied Thermal Engineering 2010;30:760–9.
[17] Madhawa Hettiarachchi HD, Golubovic M, Worek WM, Ikegami Y. Optimum design criteria for an organic Rankine cycle using low-temperature geothermal heat sources. Energy 2007;32:1698–706.
[18] Roy JP, Mishra MK, Misra A. Performance analysis of an organic Rankine cycle with superheating under different heat source. Applied Energy 2011;88: 2995–3004.
[19] Aljundi IH. Effect of dry hydrocarbons and critical point temperature on the efficiencies of organic Rankine cycle. Renewable Energy 2011;36:1196–202.
[20] Schuster A, Karellas S, Aumann R. Efficiency optimization potential in supercritical organic Rankine cycles. Energy 2010;35:1033–9.
[21] Chen H, Goswami DY, Rahman MM, Stefanakos EK. A supercritical Rankine cycle using zeotropic mixture working fluids for the conversion of low-grade heat into power. Energy 2011;36:549–55.
[22] Incropera FP, DeWitt DP. Fundamentals of heat and mass transfer (6th ed.). Wiley.
[23] Butterworth D. Developments in the design of shell and tube condenser. ASME; 1977. paper 77-WA/HT-24.
[24] Eissenberg DM. An investigation of the variable affecting steam condensation on the outside of a horizontal tube bundle. PhD thesis, University of Tennessee, Knoxville; 1972.
[25] Kim YS. An experimental study on evaporation heat transfer characteristics and pressure drop in plate heat exchanger. M.S. thesis, Yonsei University; 1999.
[26] Han DH, Lee KJ, Kim YH. Experiments on characteristics of evaporation of R410A in brazed plate heat exchangers with different geometric configurations. Applied Thermal Engineering 2003;23:1209–25.
[27] Somayaji C, Mago P, Chamra LM. Second law analysis and optimization of organic Rankine cycles. In: ASME power conference, paper no. PWR2006-88061, Atlanta, GA, May 2–4, 2006.
[28] Maizza V, Maizza A. Working fluids in non-steady flows for waste energy recovery systems. Applied Thermal Engineering 1996;16:579–90.
[29] Karellas S, Schuster A. Supercritical fluid parameters in organic Rankine cycle applications. International Journal of Thermodynamics 2008;11:101–8.
[30] Calm JM, Hourahan GC. Refrigerant data update. Heating, Piping, and Air Conditioning Engineering 2007;79(1):50–64.